Supplementary Information (SI) for Dalton Transactions.
This journal is © The Royal Society of Chemistry 2026

Supporting Information

Strongly Axial Monodentate Carboxylate for Dysprosium Single-Ion Magnet

Tao-Xiao Wen, Jia-Chuan Liu, Yan-Cong Chen, Shan-Nan Du, Si-Guo Wu, Wei Deng*, Jun-Liang Liu* and Ming-Liang Tong

Key Laboratory of Bioinorganic and Synthetic Chemistry of the Ministry of Education, IGCME, School of Chemistry, Sun Yat-Sen University, Guangzhou 510006, P. R. China

*Corresponding Author(s): Wei Deng: dengw55@mail.sysu.edu.cn; Jun-Liang Liu: liujliang5@mail.sysu.edu.cn

Contents

Experimental section

General procedures

All reactions and operations described below were performed under aerobic conditions. Benzothiohydrazide and H_2DABBT were synthesized as previously described.[1,2] Other reagents were commercially available and used as received without further purification. Diffraction intensities of three complexes were collected on an XtaLAB Synergy Custom diffractometer (Cu-K_α, λ = 1.54184 Å) at 100 K. The single-crystal structures were solved using intrinsic phasing methods (SHELXT) and refined by SHELXL-2018 in the Olex2 1.5 program.[3,4] The crystal data for all complexes have been deposited in the Cambridge Structural Database (CCDC 2496989, 2496988 and 2496990 for **1, 2** and **3**, respectively). The C, H, N, and S elemental analysis was carried out with an Elementar Vario-ELCHNS elemental analyser. Powder X-ray diffraction (PXRD) patterns were performed on a RIGAKU D-MAX 2200 VPC (*Cu-Kα*). Thermogravimetric analysis (TGA) was carried out on a NETZSCH TG209F3 thermogravimetric analyser. Infrared spectra (IR) were recorded with a Thermo NICOLET 6700 spectrometer. Magnetic susceptibility measurements were collected using a Quantum Design MPMS3 SQUID VSM magnetometer. Polycrystalline samples were embedded in Vaseline to prevent torquing.

Synthesis

Synthesis of [Dy(DABBT)(ACA)(Cy_3PO)] (1)

To a methanol solution (1 mL) of $Dy(OTf)_3$ (0.05 mmol, 30 mg), the methanol solution of H_2DABBT (0.05 mmol, 2 mL), 9-anthracenecarboxylic acid (0.05 mmol, 11mg), and tricyclohexylphosphine oxide (0.05 mmol, 15 mg) were added. Then the mixture was stirred to completely dissolve and added with triethylamine (0.15 mmol, 21 μL). The resulting solution was transferred to a Teflon-lined stainless-steel autoclave and heated at 75 °C for 48 hours. After cooling to room temperature at 5 °C h^{-1}, orange crystals suitable for X-ray diffraction were obtained and collected (32.9 mg, yield 58.34 % based on Dy). Elemental analysis for **1** ($C_{56}H_{61}DyN_5O_3PS_2$): Calc (%) C 60.61, H 5.54, N 6.31, S 5.78. Found (%) C 60.29, H 5.53, N 6.49, S 5.67. IR (ATR, cm^{-1}): 2926(w), 1631(m), 1475(s), 1398(s), 1309(m), 1223(m), 1096(vs), 922(w), 765(vs), 544(w).

Synthesis of [Dy(DABBT)(Cy_3PO)$_2$](BPh_4) (2)

To a methanol solution (1 mL) of $Dy(OTf)_3$ (0.05 mmol, 30 mg), the methanol solution of H_2DABBT (0.05 mmol, 2 mL), tricyclohexylphosphine oxide (0.05 mmol, 15 mg), [$HNEt_3$][BPh_4] (0.1 mmol, 42 mg) were added. Then the mixture was stirred to completely dissolve and added with triethylamine (0.1 mmol, 14 μL). The resulting solution

was transferred to a Teflon-lined stainless-steel autoclave and heated at 75 °C for 48 hours. After cooling to room temperature at 5 °C h^{-1}, orange crystals suitable for X-ray diffraction were obtained and collected (53.5 mg, yield 71.1 % based on Dy). Elemental analysis for **2** ($C_{83}H_{105}BDyN_5O_2P_2S_2$): Calc (%) C 66.28, H 7.03, N 4.66, S 4.26. Found (%) C 66.12, H 6.87, N 4.71, S 4.32. IR (ATR, cm^{-1}): 2931(w), 1477(m), 1447(w), 1400(m), 1227(w), 1089(vs), 1030(m), 767(w), 733(s), 704(vs), 611(s), 534(m).

Synthesis of [Dy(DABBT)(Ph_3PO)(4-Me-PhO)]·H_2O (3)

To a methanol solution (1 mL) of $Dy(OTf)_3$ (0.05 mmol, 30 mg), the methanol solution of H_2DABBT (0.05 mmol, 2 mL), triphenylphosphine oxide (0.05 mmol, 14 mg), and *p*-methylphenol (0.05 mmol, 5.4 mg) were added. Then the mixture was stirred to completely dissolve and added with triethylamine (0.15 mmol, 21 μL). The resulting solution was filtered and kept still for volatilization. Orange crystals suitable for X-ray diffraction were obtained in a few days (30.5 mg, yield 62.3 % based on Dy). Elemental analysis for **3** ($C_{48}H_{43}DyN_5O_3PS_2$): Calc (%) C 57.91, H 4.35, N 7.04, S 6.44. Found (%) C 57.71, H 4.31, N 7.36, S 6.68. IR (ATR, cm^{-1}): 1501(m), 1472(w), 1403(w), 1295(m), 1225(w), 1160(s), 1122(w), 807(m), 770(m), 724(s), 692(vs), 538(vs).

Theoretical calculation

***Ab initio* calculations**

All *ab initio* calculations are carried out with OpenMOLCAS version 20.1 and are of the CASSCF/RASSI type. The Cholesky decomposition threshold is set to 1×10^{-8} to save disk space. The entire molecules except for the solvents and the counterions are used for calculation and the atomic coordinates are extracted from the experimentally determined single-crystal structures. Active space of the CASSCF includes nine electrons in seven 4f orbitals of Dy(III), and 21 sextets for Dy(III) are optimized in state-averaged calculations and then mixed by spin-orbit coupling using RASSI approach[5]. The *g*-tensors and energies are obtained by the SINGLE_ANISO routine. The ANO-RCC basis sets[6-8] were employed for **1**, **2** ,**3**: Dy. ANO-RCC-VTZP, S. ANO-RCC-VDZP, P. ANO-RCC-VDZP, N. ANO-RCC-VDZP, O. ANO-RCC-VDZP, C. ANO-RCC-VDZ, H. ANO-RCC-VDZ.

Partial charge calculations

All quantum chemical calculations were performed using the Gaussian 09 and Multiwfn software.[9,10] The molecular geometries of the ligands (Ph_3PO, Cy_3PO, ACA^-, *p*-methylphenol) and the atomic coordinates are extracted from the experimentally determined single-crystal structures. Partial charge calculations were based on B3LYP in conjunction with the 6-311G(d, p) basis set. CHELPG, MK and RESP methods are employed to derive atomic partial charges.[11-13]

Crystal Data and Structures

Table S1. Crystallographic data and structural refinements for **1**, **2** and **3**.

	1	**2**	**3**
Empirical formula	$C_{56}H_{61}DyN_5O_3PS_2$	$C_{83}H_{105}BDyN_5O_2P_2S_2$	$C_{48}H_{43}DyN_5O_3PS_2$
Formula weight	1103.64	1504.08	995.46
Temperature / K	100.00(10)	100.00(10)	100.01(10)
Crystal system	monoclinic	monoclinic	triclinic
Space group	$P2_1/c$	$P2_1/c$	$P\bar{1}$
***a* / Å**	9.73050(10)	19.0610(2)	9.88750(10)
***b* / Å**	23.5563(3)	22.3098(2)	13.4559(2)
***c* / Å**	23.6344(4)	19.3467(2)	16.7263(2)
α / °	90	90	84.4600(10)
β / °	93.1400(10)	113.7300(10)	88.0500(10)
γ / °	90	90	79.3970(10)
Volume / Å^3	5409.22(13)	7531.54(14)	2176.84(5)
Z	4	4	2
ρ_{calc} / g cm^{-3}	1.355	1.326	1.519
μ / mm^{-1}	8.753	6.609	10.808
***F*(000)**	2252	3148	1006
Crystal size / mm^3	0.08 × 0.05 × 0.02	0.1 × 0.1 × 0.03	0.2 × 0.07 × 0.04
Radiation	Cu K_α (λ = 1.54184)	Cu K_α (λ = 1.54184)	Cu K_α (λ = 1.54184)
2Θ range for data collection / °	5.3 to 155.85	5.064 to 155.794	5.308 to 148.856
Index ranges	$-11 \le h \le 12$, $-29 \le k \le 20$, $-29 \le l \le 29$	$-24 \le h \le 23$, $-24 \le k \le 28$, $-24 \le l \le 24$	$-12 \le h \le 9$, $-16 \le k \le 16$, $-20 \le l \le 19$
Reflections collected	44605	60120	22153
Independent reflections	11369 [R_{int} = 0.0388, R_{sigma} = 0.0357]	15826 [R_{int} = 0.0338, R_{sigma} = 0.0308]	8381 [R_{int} = 0.0440, R_{sigma} = 0.0450]
Data/restraints/ parameters	11369/0/709	15826/0/1188	8381/1/535
Goodness-of-fit on F^2	1.101	1.032	1.073
Final *R* indexes [*I* >= 2σ(*I*)][a]	R_1 = 0.0510, wR_2 = 0.1188	R_1 = 0.0401, wR_2 = 0.1024	R_1 = 0.0420, wR_2 = 0.1143
Final *R* indexes [all data]	R_1 = 0.0547, wR_2 = 0.1205	R_1 = 0.0441, wR_2 = 0.1050	R_1 = 0.0450, wR_2 = 0.1161
Largest diff. peak/hole / e Å^{-3}	0.66/−1.28	1.31/−1.00	2.11/−1.19
CCDC number	2496989	2496988	2496990

[a] $R_1 = \Sigma||F_o| - |F_c||/\Sigma|F_o|$. $w_{R2} = [\Sigma w(F_o^2 - F_c^2)^2/\Sigma w(F_o^2)^2]^{1/2}$.

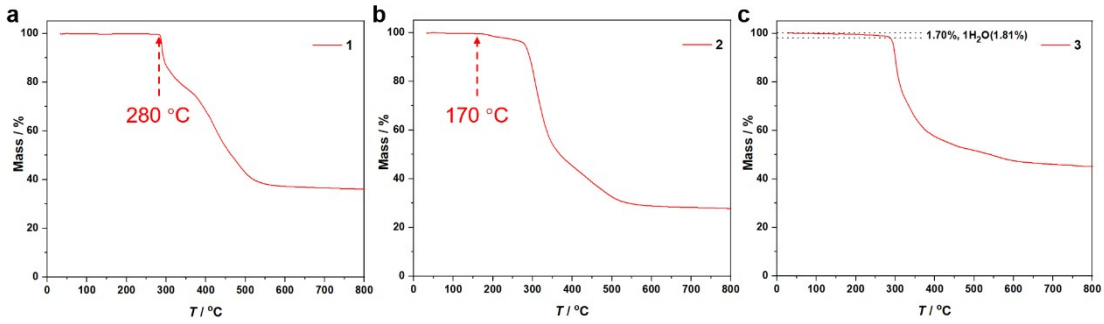

Figure S1. Thermogravimetric analysis of **1** (a), **2** (b), and **3** (c). The black dashed line in Figure (c) shows the stage due to the escape of solvent molecules.

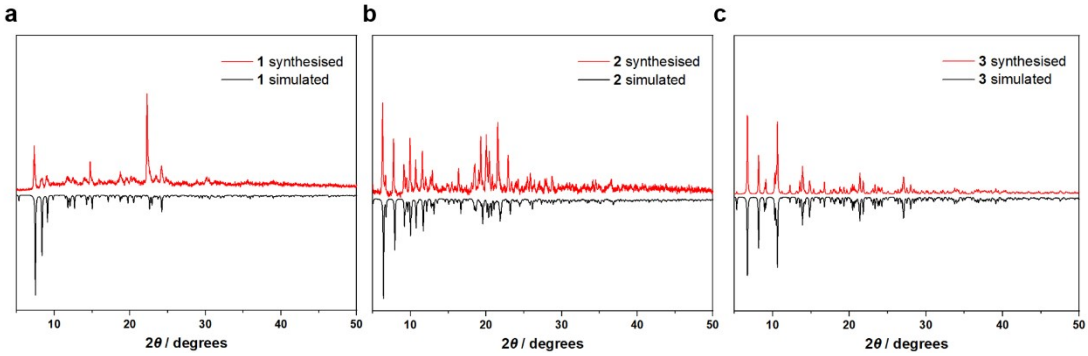

Figure S2. PXRD patterns of **1**, **2**, and **3** compared with the simulated pattern from the single crystal structure.

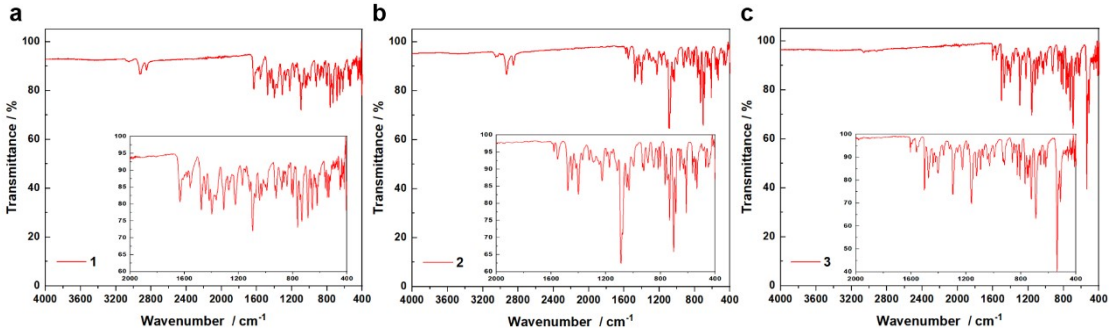

Figure S3. Attenuated total reflectance Fourier-transform infrared spectra (ATR-IR) for **1**, **2**, and **3**.

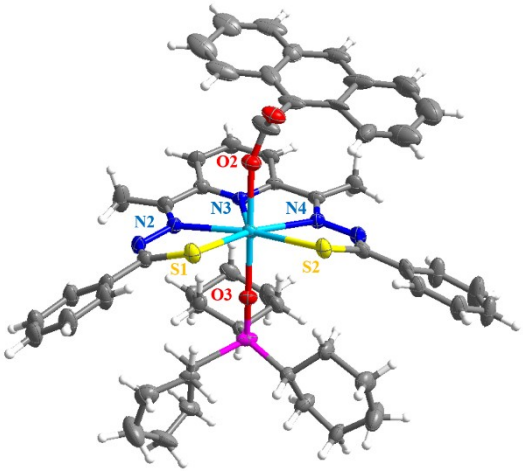

Figure S4. The asymmetric unit for **1**. Thermal ellipsoids are at the 50% probability level. Colour codes: sky blue (Dy), yellow(S), purple(P), grey (C), red (O), blue (N), white (H). The disordered parts of ACA^{-} and Cy_3PO are omitted for clarity.

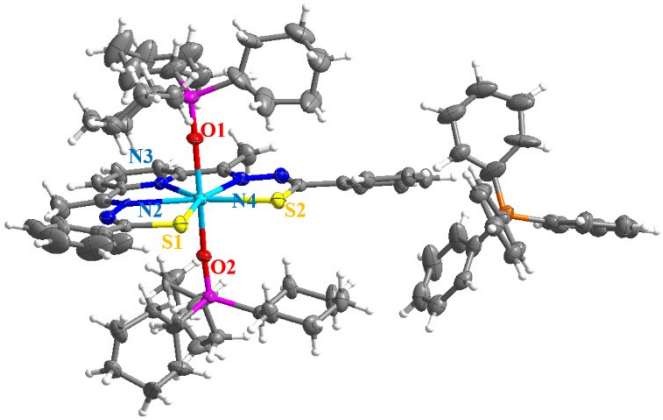

Figure S5. The asymmetric unit for **2**. Thermal ellipsoids are at the 50% probability level. Colour codes: sky blue (Dy), yellow(S), purple(P), orange(B), grey (C), red (O), blue (N), white (H). The disordered parts of $DABBT^{2-}$ and Cy_3PO are omitted for clarity.

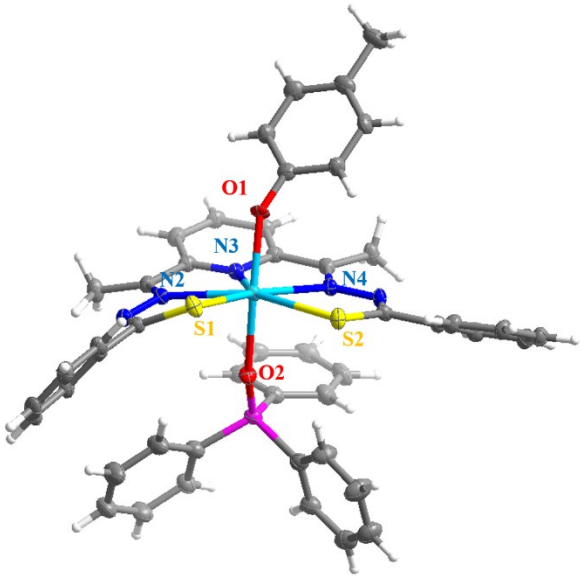

Figure S6. The asymmetric unit for **3**. Thermal ellipsoids are at the 50% probability level. Colour codes: sky blue (Dy), yellow (S), purple (P), grey (C), red (O), blue (N), white (H).

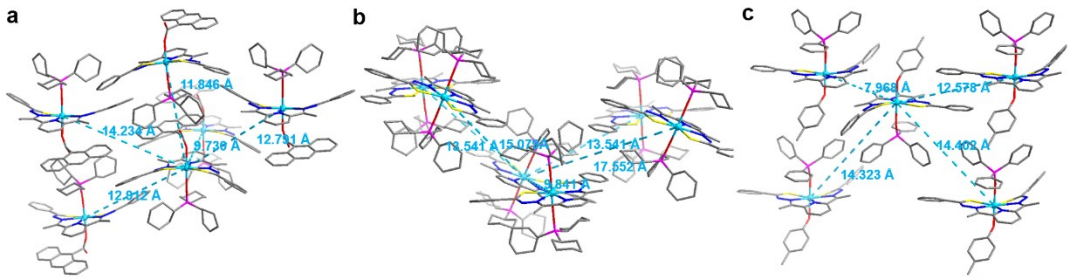

Figure S7. The crystal packing diagrams of **1** (a), **2** (b), and **3** (c). Sky blue dashed lines indicate the distance between surrounding Dy atoms. The BPh_4^- units of **2** and disordered parts are omitted for clarity.

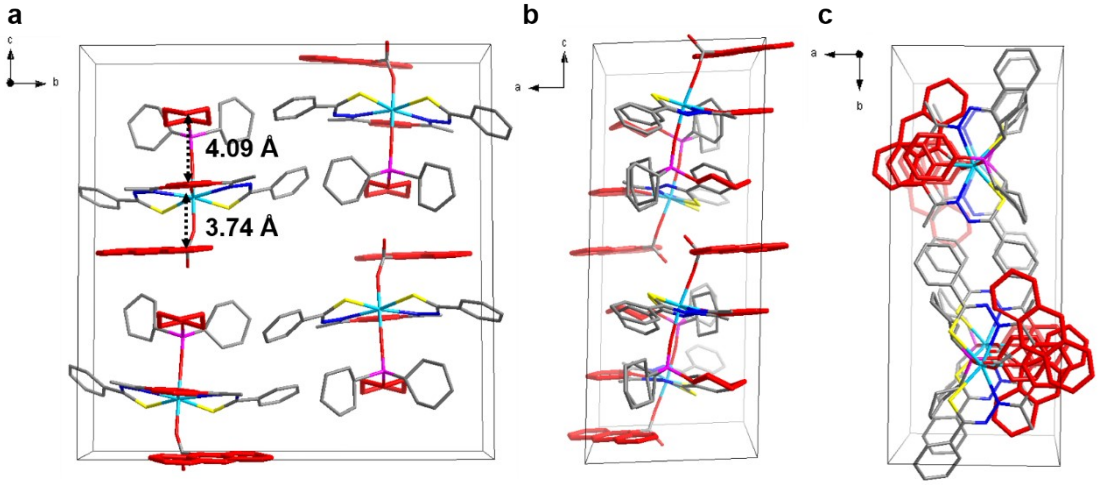

Figure S8. The crystal packing diagram in a unit cell of **1** along *a* (a), *b* (b) and *c* (c) axis. Anthracene rings, Cyclohexyl on the phosphine oxide ligand, and the pyridine rings of $DABBT^{2-}$ are highlighted. The disordered parts are omitted for clarity.

Table S2. Continuous shape measures calculations (*CShM*) for Dy(III) for **1**, **2** and **3**.[14,15]

Complex	HP-7 (D_{7h})	HPY-7 (C_{6v})	PBPY-7 (D_{5h})	COC-7 (C_{3v})	CTPR-7 (C_{2v})	JPBPY-7 (D_{5h})	JETPY-7 (C_{3v})
1	32.225	22.814	2.161	7.389	6.059	3.224	23.896
2	32.350	22.915	1.732	8.711	6.746	2.734	23.682
3	32.555	24.809	2.174	7.683	6.246	3.295	23.271

*HP-7 = Heptagon; HPY-7 = Hexagonal pyramid; PBPY-7 = Pentagonal bipyramid; COC-7 = Capped octahedron; CTPR-7 = Capped trigonal prism; JPBPY-7 = Johnson pentagonal bipyramid; JETPY-7 = Johnson elongated triangular pyramid.

Table S3. The selected bond lengths (Å) and bond angles (°) for **1**, **2**, and **3**.

1		**2**		**3**	
Dy1−O2	2.179(3)	Dy1−O1	2.2144(18)	Dy1−O1	2.139(3)
Dy1−O3	2.213(3)	Dy1−O2	2.2122(16)	Dy1−O2	2.294(3)
Dy1−S1	2.7602(10)	Dy1−S1 Dy1−S1A	2.712(7) 2.796(10)	Dy1−S1	2.7554(9)
Dy1−S2	2.7649(10)	Dy1−S2 Dy1−S2A	2.705(2) 2.823(3)	Dy1−S2	2.7541(10)
Dy1−N2	2.471(3)	Dy1−N2 Dy1−N2A	2.409(19) 2.57(3)	Dy1−N2	2.475(3)
Dy1−N3	2.429(3)	Dy1−N3 Dy1−N3A	2.494(18) 2.36(3)	Dy1−N3	2.409(3)
Dy1−N4	2.478(3)	Dy1−N4 Dy1−N4A	2.533(9) 2.390(13)	Dy1−N4	2.488(3)
O2−Dy1−O3	173.15(11)	O1−Dy1−O2	169.46(7)	O1−Dy1−O2	164.30(10)
S1−Dy1−S2	91.93(3)	S1−Dy1−S2 S1A−Dy1−S2A	90.69(16) 84.9(2)	S1−Dy1−S2	90.02(3)
S2−Dy1−N4	68.49(8)	S2−Dy1−N4 S2A−Dy1−N4A	70.2(2) 69.3(2)	S2−Dy1−N4	68.49(8)
N4−Dy1−N3	65.88(11)	N4−Dy1−N3 N4A−Dy1−N3A	65.2(3) 67.5(4)	N4−Dy1−N3	66.59(10)
N3−Dy1−N2	65.71(11)	N3−Dy1−N2 N3A−Dy1−N2A	59.9(4) 74.5(6)	N3−Dy1−N2	66.39(10)
N2−Dy1−S1	68.84(8)	N2−Dy1−S1 N2A−Dy1−S1A	73.9(4) 64.0(6)	N2−Dy1−S1	69.37(8)

Magnetic Characterization

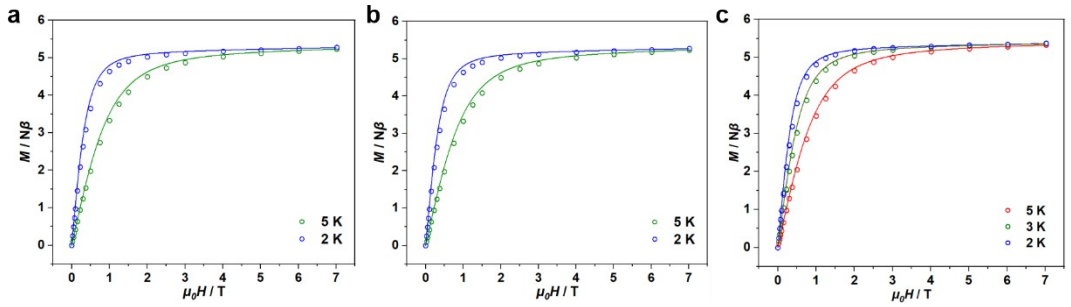

Figure S9. Variable-field magnetization data for **1** (a), **2** (b), and **3** (c). Data were collected from 0 to 7 T under steady fields. The solid lines correspond to the *ab initio* calculations.

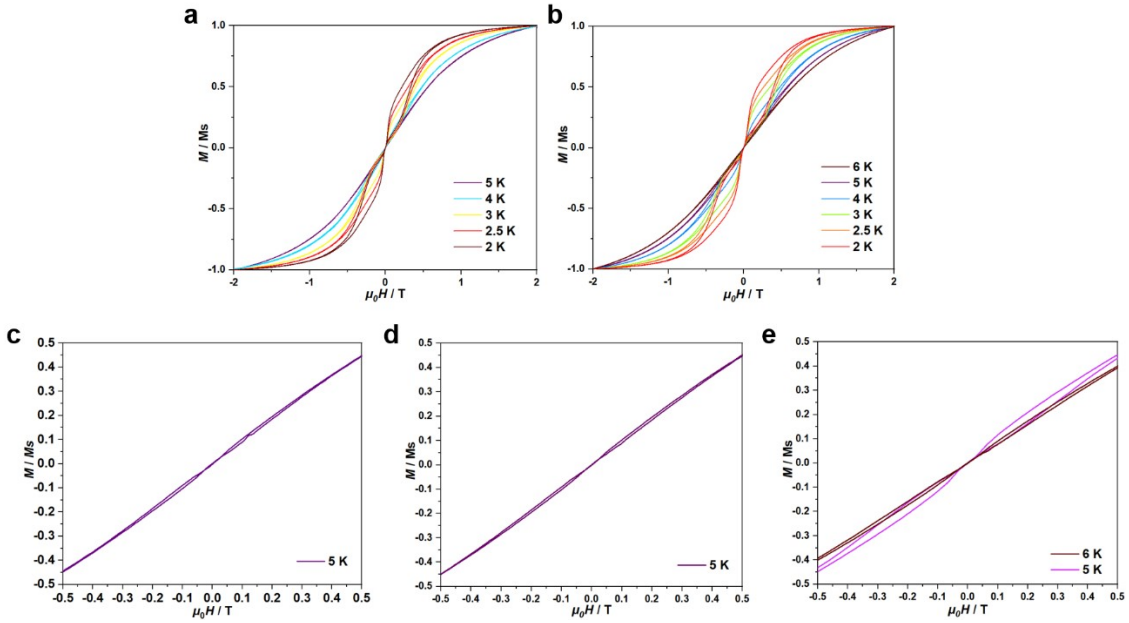

Figure S10. Normalized magnetic hysteresis loops for **2** (a) and **3** (b). Normalized magnetic hysteresis loops of **1** (c) and **2** (d) measured at 5 K, and of **3** (e) measured at 5 and 6 K. The data were continuously collected with a sweep rate of 200 Oe/s.

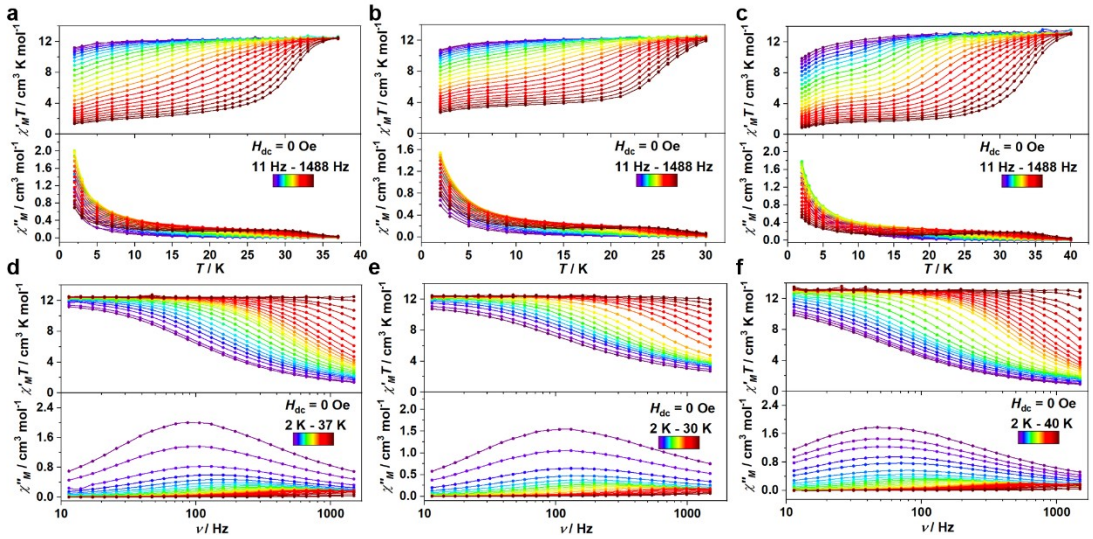

Figure S11. Temperature dependence and frequency dependence of the in-phase χ'_M and out-of-phase χ''_M under 0 field for **1** (a and d), **2** (b and e), and **3** (c and f). The solid lines are guides for the eyes.

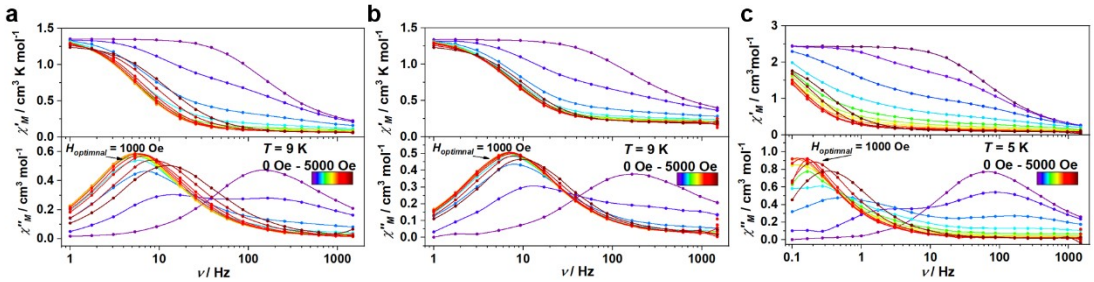

Figure S12. Frequency dependence of ac magnetic susceptibilities at 9 K, 9 K, 5 K for **1** (a), **2** (b), and **3** (c), respectively. The solid lines are guides for the eyes. The optimal applied dc field for three complexes was 1000 Oe.

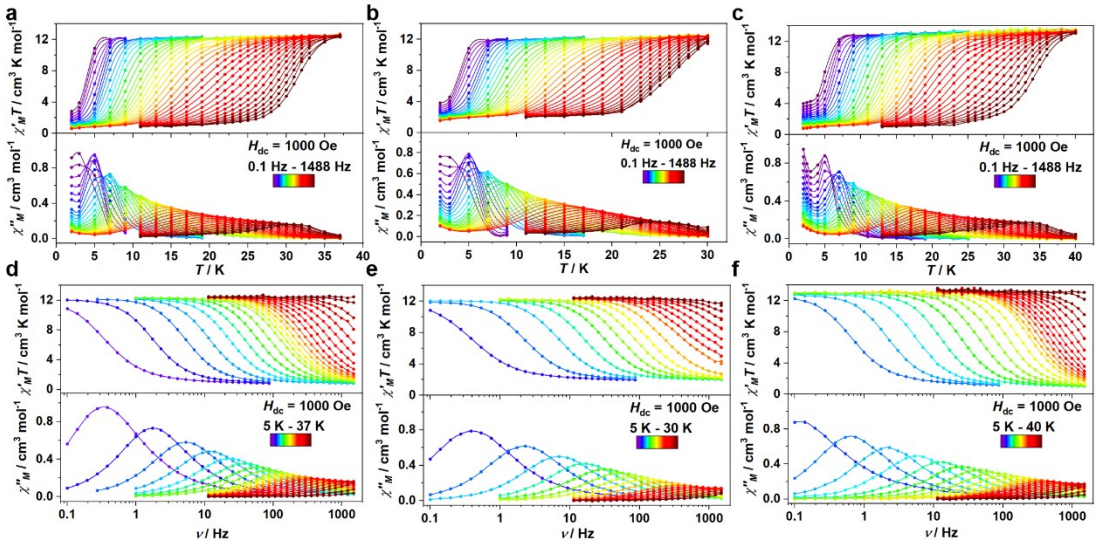

Figure S13. Temperature dependence and frequency dependence of the in-phase χ'_M and out-of-phase χ''_M under 1000 Oe dc field for **1** (a and d), **2** (b and e), and **3** (c and f). The solid lines are guides for the eyes.

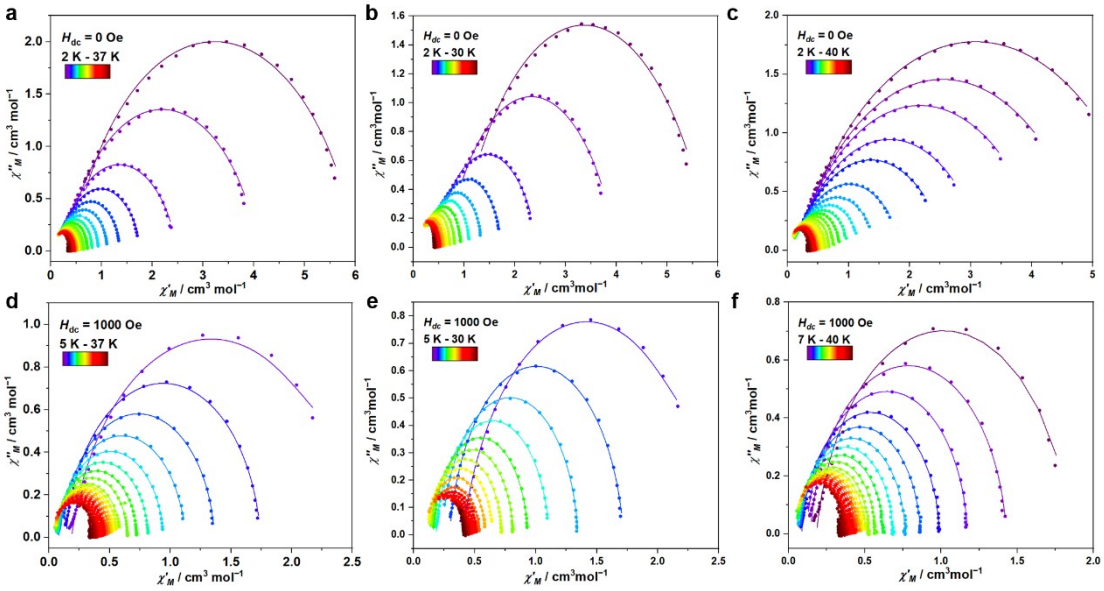

Figure S14. Cole-Cole plot under 0 and 1000 Oe dc field for **1** (a and d), **2** (b and e), and **3** (c and f). The solid lines are the best fit for generalized Debye model (**1**: α = 0.080 ~ 0.297 for H_{dc} = 0 Oe from 2 to 30 K and α = 0.052 ~ 0.175 for H_{dc} = 1000 Oe from 5 to 30 K, **2**: α = 0.038 ~ 0.214 for H_{dc} = 0 Oe from 2 to 37 K and α = 0.030 ~ 0.065 for H_{dc} = 1000 Oe from 5 to 37 K, **3**: α = 0.051 ~ 0.306 for H_{dc} = 0 Oe from 2 to 40 K and α = 0.045 ~ 0.110 for H_{dc} = 1000 Oe from 7 to 40 K).

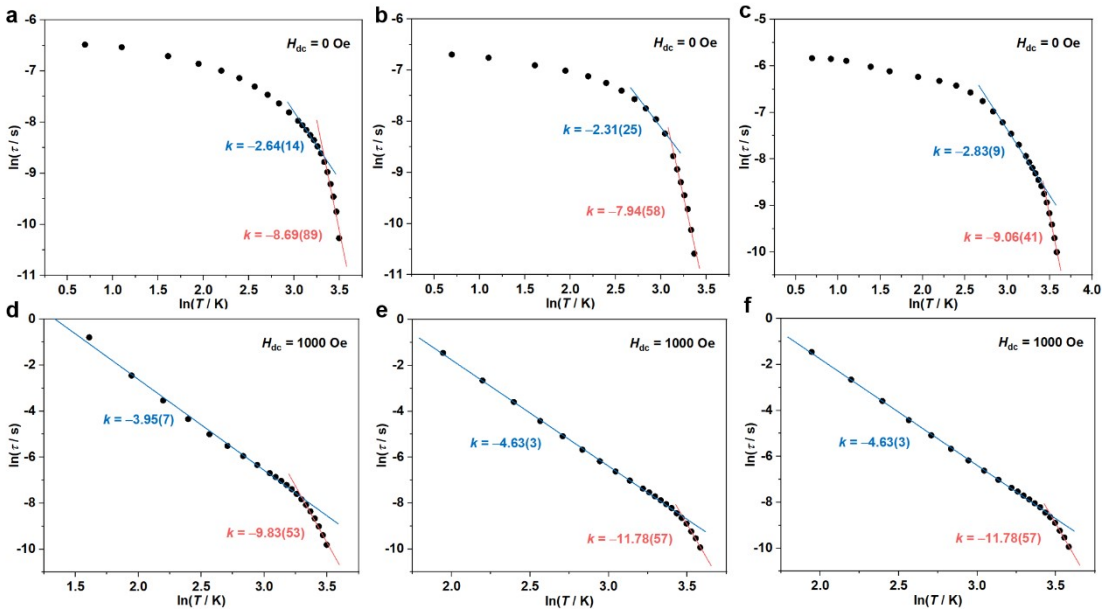

Figure S15. ln(τ) versus ln(*T*) for **1** (a and d), **2** (b and e), and **3** (c and f) under 0 and 1000 Oe dc field. A clear crossover is observed in the high-temperature region in each plot, indicating the presence of an Orbach relaxation process in all three complexes. The solid lines represent the fitting curves corresponding to the Raman and Orbach processes.

Ab initio calculations

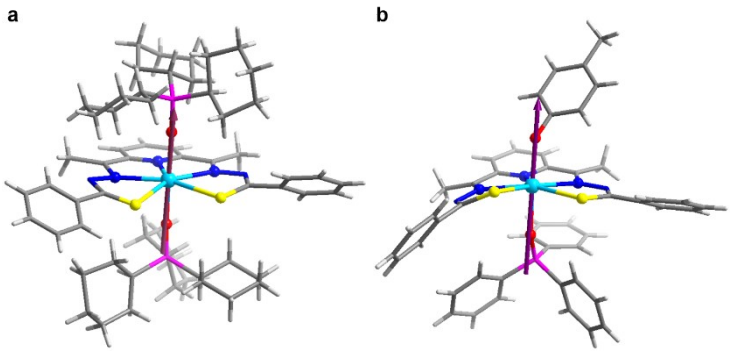

Figure S16. Molecular structures for *ab initio* calculations for **2** (a) and **3** (b). Colour code: sky blue (Dy), yellow(S), purple(P), grey (C), red (O), blue (N), white (H). The plum lines with arrows represent the calculated orientations of the local main magnetic axes.

Table S4. *Ab initio* calculated results for the $^6H_{15/2}$ multiplet of Dy(III) for **1**.

KD	E / cm^{-1}	g_x	g_y	g_z	Wavefunction
1	0	0.008	0.011	19.947	99.8%|±15/2>+0.2%|±9/2>
2	280.6	1.043	2.472	15.240	87.6%|±13/2>+9.0%|±1/2>+1.7%|±3/2>
3	340.3	0.461	1.592	16.560	50.6%|±1/2>+23.4%|±3/2>+9.2%|±13/2>
4	411.5	3.479	6.631	10.465	50.6%|±3/2>+19.9%|±11/2>+6.7%|±5/2>
5	457.7	8.883	6.898	1.731	47.3%|±5/2>+18.2%|±7/2>+12.2%|±1/2>
6	489.0	0.643	3.766	9.422	59.2%|±11/2>+12.6%|±5/2>+7.3%|±1/2>
7	552.1	3.269	5.979	11.277	57.6%|±9/2>+33.0%|±7/2>+5.0%|±11/2>
8	627.4	0.437	0.858	17.903	30.1%|±7/2>+21.2%|±5/2>+13.0%|±3/2>

Table S5. *Ab initio* calculated results for the $^6H_{15/2}$ multiplet of Dy(III) for **2**.

KD	E / cm^{-1}	g_x	g_y	g_z	Wavefunction
1	0	0.024	0.042	19.921	99.6%|±15/2>+0.1%|±11/2>+0.1%|±7/2>
2	192.8	0.780	1.116	18.561	43.8%|±1/2>+25.0%|±3/2>+12.6%|±5/2>
3	279.4	0.610	2.134	14.444	84.0%|±13/2>+8.9%|±3/2>+1.3%|±7/2>
4	327.4	0.791	1.682	17.000	26.4%|±3/2>+24.1%|±1/2>+18.5%|±5/2>
5	401.0	1.235	2.838	8.819	24.5%|±11/2>+21.9%|±5/2>+21.6%|±3/2>
6	435.9	1.696	4.906	11.918	32.3%|±11/2>+29.9%|±5/2>+17.6%|±1/2>
7	488.2	7.922	5.535	1.829	43.3%|±7/2>+29.2%|±11/2>+20.0%|±9/2>
8	523.8	12.05	7.927	1.835	55.6%|±9/2>+22.5%|±7/2>+5.1%|±3/2>

Table S6. *Ab initio* calculated results for the $^6H_{15/2}$ multiplet of Dy(III) for **3**.

KD	E / cm^{-1}	g_x	g_y	g_z	Wavefunction
1	0	0.004	0.005	19.965	99.8%|±15/2>+0.2%|±3/2>
2	298.2	0.533	0.726	16.729	95.3%|±13/2>+2.5%|±1/2>+1.4%|±11/2>
3	418.9	0.945	1.184	15.937	50.5%|±1/2>+21.6%|±3/2>+12.7%|±11/2>
4	473.1	3.857	5.883	8.758	40%|±11/2>+38.1%|±3/2>+11.3%|±9/2>
5	506.4	0.092	2.511	11.880	57.3%|±5/2>+12.9%|±3/2>+12.3%|±11/2>
6	521.9	1.876	3.341	9.084	25.2%|±11/2>+24.3%|±7/2>+24.3%|±1/2>
7	592.2	2.882	4.362	12.089	50.1%|±9/2>+22.7%|±7/2>+8.9%|±11/2>
8	645.4	0.744	2.182	17.432	34.5%|±7/2>+22.6%|±5/2>+19.6%|±9/2>

Table S7. Weight of individual crystal field parameters (CFs) on the crystal field splitting of three complexes, where the CFs are given in extended Stevens operators (ESO) and irreducible tensor operators (ITO).[16]

k	q	1			2		
		B_k^q / cm^{-1} (ESO)	B_k^q / cm^{-1} (ITO)	Weight (in%)	B_k^q / cm^{-1} (ESO)	B_k^q / cm^{-1} (ITO)	Weight (in%)
2	−2	−4.6277E−01	−3.7785E−01	3.71	−8.9024E−01	−7.2688E−01	7.48
2	−1	−2.7490E−02	−1.1220E−02	0.11	1.5127E+00	6.1755E−01	6.36
2	0	−2.1676E+00	−2.1676E+00	21.31	−1.5077E+00	−1.5077E+00	15.52
2	1	−4.8183E−01	−1.9670E−01	1.93	5.9315E−01	2.4215E−01	2.49
2	2	−1.2660E+00	−1.0337E+00	10.16	1.6267E+00	1.3282E+00	13.67
4	−4	3.6600E−03	8.7450E−04	1.56	7.5016E−04	1.7932E−04	0.33
4	−3	2.8730E−02	2.4300E−03	4.33	−3.1600E−03	−2.6742E−04	0.50
4	−2	3.9602E−04	1.2523E−04	0.22	−3.3242E−04	−1.0512E−04	0.20
4	−1	−4.7920E−04	−1.0715E−04	0.19	−8.5000E−03	−1.9000E−03	3.55
4	0	−1.0950E−02	−1.0950E−02	19.53	−1.0910E−02	−1.0910E−02	20.39
4	1	1.3700E−03	3.0735E−04	0.55	−1.6700E−03	−3.7416E−04	0.70
4	2	6.2800E−03	1.9900E−03	3.54	−4.6700E−03	−1.4800E−03	2.76
4	3	−7.5300E−03	−6.3662E−04	1.14	2.4500E−03	2.0666E−04	0.39
4	4	8.8200E−03	2.1100E−03	3.76	−1.0840E−02	−2.5900E−03	4.84
6	−6	−2.8382E−04	−3.7348E−05	6.25	8.8569E−06	1.1655E−06	0.20
6	−5	−3.7408E−05	−1.4210E−06	0.24	6.1135E−05	2.3223E−06	0.41
6	−4	1.5160E−05	2.7011E−06	0.45	1.3034E−06	2.3224E−07	0.04
6	−3	1.4995E−04	1.4634E−05	2.45	−1.9560E−06	−1.9089E−07	0.03
6	−2	2.1676E−05	4.2308E−06	0.71	−1.1992E−05	−2.3407E−06	0.41
6	−1	5.1790E−06	7.9914E−07	0.13	−3.7183E−05	−5.7375E−06	1.01
6	0	1.4890E−05	1.4890E−05	2.49	7.8378E−06	7.8378E−06	1.37
6	1	3.3556E−05	5.1778E−06	0.87	−4.2163E−05	−6.5059E−06	1.14
6	2	−9.5406E−06	−1.8621E−06	0.31	−2.2820E−05	−4.4539E−06	0.78
6	3	−4.5944E−05	−4.4837E−06	0.75	1.4595E−05	1.4244E−06	0.25
6	4	4.4943E−05	8.0077E−06	1.34	−8.9094E−05	−1.5874E−05	2.78
6	5	−7.6731E−05	−2.9148E−06	0.49	−4.3168E−04	−1.6398E−05	2.87
6	6	−4.0753E−04	−5.3627E−05	8.97	3.1726E−04	4.1748E−05	7.31

k	q	3		
		B_k^q / cm^{-1} (ESO)	B_k^q / cm^{-1} (ITO)	Weight (in %)
2	−2	1.5041E−01	1.2281E−01	1.22
2	−1	2.4253E−01	9.9010E−02	0.99
2	0	−2.6096E+00	−2.6096E+00	26.01
2	1	1.0723E+00	4.3778E−01	4.36
2	2	−8.9123E−01	−7.2769E−01	7.25
4	−4	−4.2800E−03	−1.0200E−03	1.85
4	−3	−1.0440E−02	−8.8239E−04	1.60
4	−2	8.5179E−04	2.6936E−04	0.49
4	−1	−3.6700E−03	−8.2087E−04	1.48
4	0	−1.0160E−02	−1.0160E−02	18.37
4	1	−1.5500E−03	−3.4621E−04	0.63
4	2	6.0200E−03	1.9000E−03	3.44
4	3	1.4300E−03	1.2082E−04	0.22
4	4	5.0500E−03	1.2100E−03	2.18
6	−6	1.8337E−04	2.4130E−05	4.09
6	−5	2.1953E−04	8.3394E−06	1.41
6	−4	−3.8415E−05	−6.8446E−06	1.16
6	−3	−8.2951E−05	−8.0952E−06	1.37
6	−2	4.4501E−05	8.6856E−06	1.47
6	−1	4.6041E−05	7.1043E−06	1.21
6	0	9.7868E−06	9.7868E−06	1.66
6	1	−1.0756E−04	−1.6596E−05	2.81
6	2	−4.4405E−05	−8.6670E−06	1.47
6	3	2.3581E−05	2.3013E−06	0.39
6	4	−4.2846E−06	−7.6340E−07	0.13
6	5	1.7129E−04	6.5068E−06	1.10
6	6	−4.0208E−04	−5.2910E−05	8.97

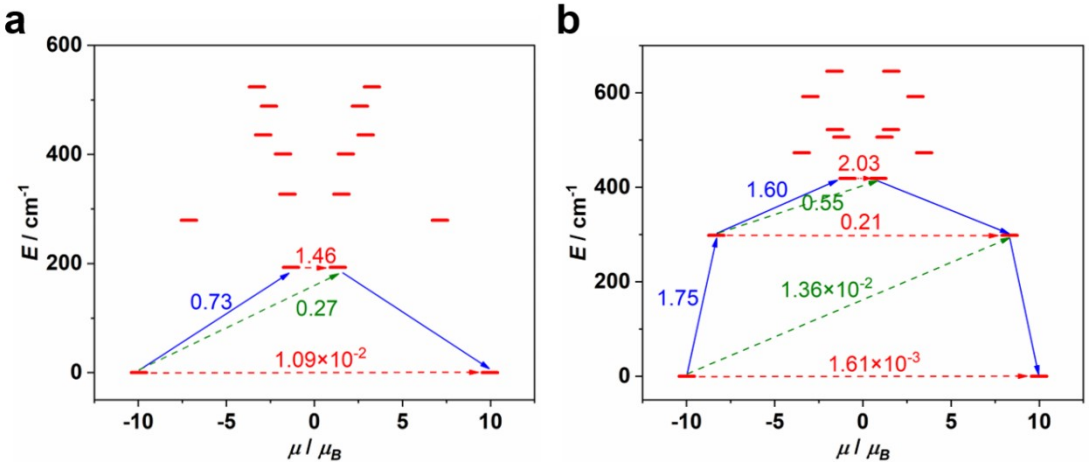

Figure S17. Probability of the relaxation process for **2** (a) and **3** (b). The thick red lines represent the low-lying KDs as a function of their magnetic moment along the magnetic axis. The red dashed lines correspond to QTM; the green and blue lines represent the spin-phonon transitions. The numbers at each arrow stand for the average matrix element of the magnetic moment.

Table S8. Calculated CHELPG, MK and RESP charges (a.u.) of O atoms in isolated ligands based on DFT calculations.

	Cy_3PO	ACA^-	*p*-methylphenol	Ph_3PO
CHELPG	−0.7144	−0.8186	−0.9196	−0.6651
MK	−0.6664	−0.7757	−0.9300	−0.6728
RESP	−0.6668	−0.7744	−0.9276	−0.6705

Table S9. Comparison of structural and magnetic parameters for Dy-SMMs with monodentate carboxylate.

Compound	Dy–O(carboxylate) bond length (Å)	Local pseudo-symmetry	U_{eff} (0 Oe, cm^{-1})	τ_0 (s)	Ref.
$[(\mu_3\text{-}C_9H_3O_6)\{L^1CuDy\text{-}(NO_3)_2\}_3]$	2.312	C_{4v}	n.a.	n.a.	17
$(HDABCO)_8H_5Li_8[Dy_4As_5W_{40}O_{144}(H_2O)_{10}(gly)_2]\cdot 25H_2O$	2.269	D_{4d}	2.8	1.9×10^{-5}	18
$[C(NH_2)_3]_{11}[Dy_2(Hcit)_2(AsW_{10}O_{38})]\cdot 9H2O$	2.332-2.483	C_{2v}	38	2.0×10^{-9}	19
$[Dy(H_3L^2)_2](NO_3)\cdot EtOH\cdot 8H_2O$	2.324, 2.358	D_{4d}	42	4.4×10^{-11}	20
$(HNEt_3)[Dy(bpyda)_2]\cdot 3H_2O$	2.305-2.350	D_{2d}	38	n.a.	21
$Me_4N[Dy(HL^3)_4]\cdot 2CH_3CN$	2.340-2.373	D_{2d}	50–65	$(2.06–4.35)\times10^{-10}$	22
$[Dy_4(HL^4)_2(L)_4(\mu_3\text{-}OH)_2]\cdot 5(MeOH)_2\cdot 7H_2O$	2.239, 2.300	D_{4d}	58	5.1×10^{-9}	23
$[N(CH_3)_4]_6K_3H_7[Dy(C_4H_2O_6)(\alpha\text{-}PW_{11}O_{39})]_2\cdot 27H_2O$	2.437	D_{4d}	14	4.2×10^{-7}	24
$[Dy(HL^5)_3]\cdot 8H_2O$	2.360	D_{3h}	13.6	7.0×10^{-9}	25
$[Dy(HL^6)_3]\cdot 8H_2O$	2.347	D_{3h}	24	1.6×10^{-9}	
$Dy_2(L^7)_2(DBM)_2(DMF)_2$	2.278	D_{4d}	75	2.12×10^{-9}	27
$Dy_2(L^7)_2(DBM)_2(DMA)_2$	2.281	D_{4d}	86	2.87×10^{-9}	
$Dy(PyrCOO)(acac)_2(H_2O)_2$	2.376	C_{2v}	53.5	8.3×10^{-10}	28
$[Dy_2(L^8)_2(DBM)_2(DMF)_2]\cdot 3CH_3OH$	2.292, 2.306	D_{4d}	7.6	1×10^{-5}	29
$[Cu_3Dy_2(H_3L^9)_2(OAc)_2(hfac)_4]\cdot 2MeOH$	2.358	D_{2d}	21	9.7×10^{-9}	30
$(Hpy)[DyPr(HL^{10})_3(NO_3)(py)(H_2O)]$	2.343	D_{2d}	37	2.15×10^{-6}	31
$Na[Dy(4\text{-}HOpa)_4(H_2O)]\cdot 2H_2O$	2.382-2.434	C_{4v}	11	1.4×10^{-8}	32
$Bu_4N[Dy(HL^{11})_4(dmso)]\cdot 2H_2O$	2.383-2.391	D_{4d}	n.a.	n.a.	33
$Bu_4N[Dy(HL^{12})_4(dmso)]\cdot 3H_2O$	2.363-2.392	D_{4d}			
$Dy\{Ir(ppy)_2(dcbpy)\}_2(NO_3)(H_2O)_5]\cdot solvent$	2.332	D_{2d}	3.6	7.34×10^{-5}	34
$[Dy_2(L^{13})_2(dbm)_2(CH_3OH)_2]\cdot 3CH_3OH$	2.321	C_{2v}	12.5 (5k Oe)	7.34×10^{-7}	35
$[Dy(H_3L^{14})(CH_3COO)_2(EtOH)]\cdot CH_3COOH$	2.281	C_s	18.4 (1k Oe)	1.03×10^{-6}	36
$[Dy_2(H_2NDISA)_3(DMF)_3(H_2O)_{10}]\cdot 1.4DMF\cdot 2.6H_2O$	2.320, 2.399	D_{2d}	n.a.	n.a.	37
Dy(DABBT)(ACA)(Cy_3PO)	2.179	D_{5h}	313	2.1×10^{-9}	**1** in this work

H_2L^1 = N,N'-bis(3-hydroxymethyl-5-methylsalicylidene)-1,3-propilendiamine; HDABCO = monoprotonated 1,4-diazabicyclooctane; gly = glycine; $Hcit^{3-}$ = $[C(OH)(COO^-)(CH_2COO^-)_2]$); H_4L^2 = 2,2'-{[(2-aminoethyl)imino]bis[2,1-ethanediyl-nitriloethylidyne]}bis-2-hydroxy-benzoic acid; oda = oxidiacetate; bpyda = 2,2'-bipyridine-6,6'-dicarboxylate; H_2L^3 = N-(2,6-dimethylphenyl)oxamic acid; H_2L^4 = (2-aminoethyl)-hydroxybenzoic acid; H_2L^5 = N-[(imidazol-4-yl)methylidene]-DL-alanine; H_2L^6 = N-[(imidazol-4-yl)methylidene]-DL-phenylalanine; H_2L^7 = 2-(2-hydroxy-3-methoxybenzylidene)hydrazine-1-carboxylic acid; $acac^-$ = acetylacetonate (pentane-2,4-dionate) anion; bipy = 4,4'-bipyridine; nb = *p*-nitrobenzoate; phen = 1,10-phenanthroline; H_2L^8 = 2-((2-hydroxy-3-methoxybenzylidene)amino)acetic acid; HDBM = dibenzoylmethane; H_6L^9 = 1,3-Bis[tris(hydroxymethyl)methylamino]propane; $hfac^-$ = hexafluoroacetylacetonate; H_3L^{10} = 6-(3-oxo-3-(2-hydroxyphenyl)propionyl)-pyridine-2-carboxylic acid; 4-HOpa = N-4-hydroxyphenyloxamate; H_2L^{11} = N-(4-

Clphenyl)oxamic acid; H_2L^{12} = N-(4-Fphenyl)oxamic acid; H_2L^{13} = 2-[[(4-methyl-2-carboxyl)imino]methyl]-8-hydroxyquinoline; H_4NDISA = N,N'-bis(3-carboxy-4-hydroxyphenyl)-1,4,5,8-naphthalenetetradicarboximide; H_4L^{14} = N',N'''-((1E,1'E)-pyridine-2,6-diylbis(ethan-1-yl-1-ylidene))bis(2-hydroxybenzohydrazide)

Reference

1 I. Ko, S. Park, G. Lee and H. Kim, *ARKIVOC*, 2019, 67-78.

2 T. -X. Wen, Z. -Y. Ruan, Y. -R. Chen, Y. -C. Chen, S. -G. Wu, S. -N. Du, W. Deng, J. -L. Liu, and M. -L. Tong, *CCS. Chem*, 2025, DOI: 10.31635/ccschem.025.202506541.

3 G. Sheldrick, *Acta Crystallogr. Sect. A*, 2008, **64**, 112−122.

4 V. Dolomanov, L. J. Bourhis, R. J. Gildea, J. A. K. Howard and H. Puschmann, *J. Appl. Crystallogr.*, 2009, **42**, 339−341.

5 P.-Å. Malmqvist, B.O. Roos and B. Schimmelpfennig. *Chem. Phys. Lett.*, 2002, **357**, 230−240.

6 B.O. Roos, R. Lindh, P.-Å. Malmqvist, V. Veryazov and P.-O. Widmark. *J Phys Chem A*, 2004, **108**, 2851−2858.

7 B.O. Roos, R. Lindh, P.-Å. Malmqvist, V. Veryazov and P.-O. Widmark. *J Phys Chem A*, 2005, **109**, 6575−6579.

8 B.O. Roos, R. Lindh, P.-Å. Malmqvist, V. Veryazov and P.-O. Widmark, A.C. Borin. *J Phys Chem A*, 2008, **112**, 11431−11435.

9 M. J. Frisch, G. W. Trucks, H. B. Schlegel, G. E. Scuseria, M. A. Robb, J. R. Cheeseman, G. Scalmani, V. Barone, G. A. Petersson, H. Nakatsuji, X. Li, M. Caricato, A. V. Marenich, J. Bloino, B. G. Janesko, R. Gomperts, B. Mennucci, H. P. Hratchian, J. V. Ortiz, A. F. Izmaylov, J. L. Sonnenberg, Williams, F. Ding, F. Lipparini, F. Egidi, J. Goings, B. Peng, A. Petrone, T. Henderson, D. Ranasinghe, V. G. Zakrzewski, J. Gao, N. Rega, G. Zheng, W. Liang, M. Hada, M. Ehara, K. Toyota, R. Fukuda, J. Hasegawa, M. Ishida, T. Nakajima, Y. Honda, O. Kitao, H. Nakai, T. Vreven, K. Throssell, J. A. Montgomery Jr., J. E. Peralta, F. Ogliaro, M. J. Bearpark, J. J. Heyd, E. N. Brothers, K. N. Kudin, V. N. Staroverov, T. A. Keith, R. Kobayashi, J. Normand, K. Raghavachari, A. P. Rendell, J. C. Burant, S. S. Iyengar, J. Tomasi, M. Cossi, J. M. Millam, M. Klene, C. Adamo, R. Cammi, J. W. Ochterski, R. L. Martin, K. Morokuma, O. Farkas, J. B. Foresman and D. J. Fox, *Gaussian 09 Rev. D.01*, 2016.

10 Lu, T. and Chen, F., *J. Comput. Chem.*,2012, **33**, 580-592.

11 B. H. Besler, K. M. Merz Jr and P. A. Kollman, *J. Comput. Chem.*, 1990, **11**, 431-439.

12 C. M. Breneman and K. B. Wiberg, *J. Comput. Chem.*, 1990, **11**, 361-373.

13 C. I. Bayly, P. Cieplak, W. Cornell and P. A. Kollman, *J. Phys. Chem.*, 1993, **97**, 10269-10280.

14 S. Alvarez, P. Alemany, D. Casanova, J. Cirera, M. Llunell and D. Avnir, *Coord. Chem. Rev.*, 2005, **249**, 1693–1708.

15 D. Casanova, M. Llunell, P. Alemany and S. Alvarez, *Chem. Eur. J.*, 2005, **11**, 1479–1494.

16 L. F. Chibotaru and L. Ungur, *J. Chem. Phys.*, 2012, **137**, 064112.

17 G. Novitchi, W. Wernsdorfer, L. F. Chibotaru, J.-P. Costes, C. E. Anson and A. K. Powell, *Angew. Chem., Int. Ed.*, 2009, **48**, 1614-1619.

18 C. Ritchie, M. Speldrich, R. W. Gable, L. Sorace, P. Kögerler and C. Boskovic, *Inorg. Chem.*, 2011, **50**, 7004-7014.

19 F. Li, W. Guo, L. Xu, L. Ma and Y. Wang, *Dalton Trans.*, 2012, **41**, 9220-9226.

20 A. Bhunia, M. T. Gamer, L. Ungur, L. F. Chibotaru, A. K. Powell, Y. Lan, P. W. Roesky, F. Menges, C. Riehn and G. Niedner-Schatteburg, *Inorg. Chem.*, 2012, **51**, 9589-9597.

21 Q.-W. Li, J.-L. Liu, J.-H. Jia, J.-D. Leng, W.-Q. Lin, Y.-C. Chen and M.-L. Tong, *Dalton Trans.*, 2013, **42**, 11262-11270.

22 F. R. Fortea-Pérez, J. Vallejo, M. Julve, F. Lloret, G. De Munno, D. Armentano and E. Pardo, *Inorg. Chem.*, 2013,

52, 4777-4779.

23 M. Yadav, V. Mereacre, S. Lebedkin, M. M. Kappes, A. K. Powell and P. W. Roesky, *Inorg. Chem.*, 2015, **54**, 773-781.

24 P. Ma, F. Hu, R. Wan, Y. Huo, D. Zhang, J. Niu and J. Wang, *J. Mater. Chem. C*, 2016, **4**, 5424-5433.

25 D. Hamada, T. Fujinami, S. Yamauchi, N. Matsumoto, N. Mochida, T. Ishida, Y. Sunatsuki, M. Tsuchimoto, C. Coletti and N. Re, *Polyhedron*, 2016, **109**, 120-128.

26 R. J. Holmberg, I. Korobkov and M. Murugesu, *RSC Adv.*, 2016, **6**, 72510-72518.

27 K. Zhang, F.-S. Guo and Y.-Y. Wang, *Dalton Trans.*, 2017, **46**, 1753-1756.

28 A. V. Gavrikov, N. N. Efimov, Z. V. Dobrokhotova, A. B. Ilyukhin, P. N. Vasilyev and V. M. Novotortsev, *Dalton Trans.*, 2017, **46**, 11806-11816.

29 K. Zhang and Y.-Y. Wang, *Inorg. Chem. Commun.*, 2017, **76**, 103-107.

30 C.-M. Liu, D.-Q. Zhang and D.-B. Zhu, *Sci. Rep.*, 2017, **7**, 15483.

31 D. Aguilà, V. Velasco, L. A. Barrios, J. González-Fabra, C. Bo, S. J. Teat, O. Roubeau and G. Aromí, *Inorg. Chem.*, 2018, **57**, 8429-8439.

32 T. T. da Cunha, V. M. M. Barbosa, W. X. C. Oliveira, C. B. Pinheiro, E. F. Pedroso, W. C. Nunes and C. L. M. Pereira, *Polyhedron*, 2019, **169**, 102-113.

33 R. C. A. Vaz, I. O. Esteves, W. X. C. Oliveira, J. Honorato, F. T. Martins, L. F. Marques, G. L. dos Santos, R. O. Freire, L. T. Jesus, E. F. Pedroso, W. C. Nunes, M. Julve and C. L. M. Pereira, *Dalton Trans.*, 2020, **49**, 16106-16124.

34 K. Fan, S.-S. Bao, R. Huo, X.-D. Huang, Y.-J. Liu, Z.-W. Yu, M. Kurmoo and L.-M. Zheng, *Inorg. Chem. Front.*, 2020, **7**, 4580-4592.

35 J. Wang, Z.-L. Wu, L.-R. Yang, M.-M. Xue, Z.-X. Fang, S.-C. Luo and W.-M. Wang, *Inorg. Chim. Acta*, 2021, **514**, 120015.

36 H.-Q. Li, Y.-C. Sun, L. Shi, F.-L. Chen, F.-X. Shen, Y. Zhao and X.-Y. Wang, *Inorg. Chem.*, 2022, **61**, 2272-2283.

37 J. -T. Chen, X. -M. Kuang, Y. -H. Li, Y. -J. Zhong, H. Zhang, J. -Y. Su, W. -B. Chen and W. Dong, *CrystEngComm*, 2024, **26**, 5461-5468.